分 类 号＿＿＿＿＿＿　　　　　　　　　学号　　D201277241

学校代码　10487　　　　　　　　　　　密级＿＿＿＿＿＿

華中科技大學

博 士 学 位 论 文

太阳能光热梯级发电系统设计及其特性研究

学位申请人：　张成

学 科 专 业：　热能工程

指 导 教 师：　高伟 教授　Inmaculada Arauzo 教授

答 辩 日 期：　2017 年 6 月 1 日

A Thesis Submitted in Partial Fulfillment of the Requirements
for the Ph.D

Cascade solar thermal power system design and research of the key features

Student : Zhang Cheng

Major : Thermal Engineering

Supervisor : Prof. Gao Wei

Prof. Inmaculada Arauzo

Huazhong University of Science & Technology

Wuhan 430074, P. R. China

June 1, 2017

独创性声明

本人声明所呈交的学位论文是我个人在导师的指导下进行的研究工作及取得的研究成果。尽我所知,除文中已标明引用的内容外,本论文不包含任何其他人或集体已经发表或撰写过的研究成果。对本文的研究做出贡献的个人和集体,均已在文中以明确方式标明。本人完全意识到本声明的法律结果由本人承担。

学位论文作者签名:

日期: 年 月 日

学位论文版权使用授权书

本学位论文作者完全了解学校有关保留、使用学位论文的规定,即:学校有权保留并向国家有关部门或机构送交论文的复印件和电子版,允许论文被查阅和借阅。本人授权华中科技大学可以将本学位论文的全部或部分内容编入有关数据库进行检索,可以采用影印、缩印或扫描等复制手段保存和汇编本学位论文。

本论文属于 保密 □,在 ____ 年解密后适用本授权书。
不保密 □。

(请在以上方框内打"√")

学位论文作者签名: 指导教师签名:

日期: 年 月 日 日期: 年 月 日

摘 要

随着化石能源的消耗和环境问题的凸显，太阳能作为一种新能源，具有分布广泛、总量巨大、取之不竭、无污染的特点，越来越受到世界各国的重视，被广泛认为是未来最有潜力替代传统化石能源的清洁能源。在发电领域，太阳能光热发电是除了太阳能光伏发电之外的另一种发电形式，与光伏发电相比，光热发电因具有发电平稳，电网兼容性友好，易于与现有化石燃料电厂组合等优点而受到越来越多的关注。

本课题属于国家国际合作项目专项“太阳能梯级集热发电系统关键技术合作研究”，本项目的目标是研究太阳能高温集热装置，提出并组建、优化太阳能梯级集热发电系统。本项目针对各种传统型式的太阳能光热发电系统的优缺点，为探索出可大规模低成本利用太阳能的光热发电技术提供新的方案。本课题通过建立各部件的机理模型，选择合理的拓扑结构，组建太阳能光热梯级集热发电系统，并建立系统的模型，针对不同的优化目标选择优化参数进行优化，最终得到低成本高效率的太阳能光热梯级发电方案，为实现高效率太阳能极热发电和大规模低成本应用提供技术支持。

首先，针对太阳能光热梯级集热发电系统的各部件建立机理模型。依据目标对象的运行机理，根据物理平衡方程，对系统中的各部件，尤其是系统中的关键部件，建立起数学模型。各部件的数学模型是经由经典理论或是大量实验数据验证的模型，是组建光热梯级集热发电系统模型的基础。其次，提出了多种太阳能光热梯级系统的拓扑结构。通过热力学分析，结合系统中各部件的工作特点，合理布局太阳能光热梯级集热发电系统，利用不同热功循环实现不同品位的能量的梯级利用。

关键词： 槽式集热器，碟式集热器，朗肯循环，斯特林循环，斯特林机组，梯级发电

Abstract

With the increasing awareness of problem of fossil energy consumption and environmental pollution, solar energy as a renewable energy, which has the advantages as widely spreeded, huge amount, inexhaustible, no pollution, has received much attention by many countries and been regarded as the greated potential candidate of the fossil energy. Concentrated solar thermal power generation is another form of power generation technology except solar photovoltaic power generation. Compared to solar photovoltaic, solar thermal power is gaining more attention for its advantages as smooth power generation, good grid compatibility, easy to combinate with existing fossil power plant.

The project of this research is an international cooperation program 'Collaborative research on key technologies to produce electricity by cascade utilization solar thermal energy'. The objective of the project is to investigate the key scientific problems related to solar heat collector in high temperature, cascade utilization solar thermal energy with high efficiency, system integration and optimization to develop the prototype system.

Key words: Parabolic trough collector, Parabolic dish collector, Rankine cycle, Stirling cycle, Stirling engine array, cascade powering

Contents

Abstract **I**

List of Figures **IX**

List of Tables **X**

1 Introduction **1**

1.1 Solar Parabolic Trough 1

1.2 Solar Parabolic dish 5

1.3 Solar Tower 7

1.4 Rankine Cycle 7

1.5 Stirling Engine 7

1.6 Brayton Cycle 9

1.7 Research Objective 9

2 System Design **10**

2.1 System Structure 10

2.2 Component Modeling 10

3 System Analysis **11**

3.1 Energy Cascade Collection 11

3.2 Energy Cascade Utilization 11

3.3 Stirling Engine Array 11

3.4 Introduction 11

3.5 Connection types of SEA 15

3.6 Thermodynamic analysis of Stirling engine 17

3.7 Modeling of the SEAs 26

3.8 Result Analysis 29

3.9 Conclusion 35

3.10 Steam Generators 36

4 Conclusions **37**
Acknowledge **38**
Bibliography **39**
Appendix A Publication **44**
Appendix B Formulae **45**

Nomenclature

A heat transfer area (m^2)

c_p specific heat at constant pressure ($J \cdot kg^{-1} \cdot K^{-1}$)

c_v specific heat at constant volume ($J \cdot kg^{-1} \cdot K^{-1}$)

e regenerator effectiveness

J annular gap cylinder displacer (m)

K dead volume factor

k specific heat ratio (c_p/c_v), thermal conductivity ($W \cdot m^{-1} \cdot K^{-1}$)

m mass of working fluid in Stirling engine (kg)

n_{se} number of Stirling engine in SEA

P power of Stirling engine (W)

p pressure (Pa)

Q absorbed heat (J)

q_m mass flow rate ($kg \cdot s^{-1}$)

R gas constant ($J \cdot kg^{-1} \cdot K^{-1}$)

s Speed of Stirling enine, Hz

s_{se} speed of Stirling engine (Hz)

T_H working fluid temperature in the hot space (K)

T_L working fluid temperature in the cold space (K)

T_R effective working fluid temperature in regenerator (K)

T_w wall temperature (K)

U overall heat transfer coefficient (W·m^{-2}·K^{-1})

V_C compression volume (m^3)

V_D total dead volume (m^3)

V_E expansion volume (m^3)

V_{DC} cold space dead volume (m^3)

V_{DH} hot space dead volume (m^3)

V_{DR} regenerator dead volume (m^3)

W output work (J)

Z displacer stroke (m)

Abbreviations

ANN Artificial Neural Network

CCHP Combined cooling, heating and power

CFD Computational Fluid Dynamics

CRTEn Reseach and Technologies Centre of Energy in Borj Cedria

DSG Direct Steam Generation

HTF Heat Transfer Fluid

LM Levenberge Marguardt

LSSVM Least squares support vector machine

MCRT Monte Carlo Ray Tracing

ORC Organic Rankine Cycle

PCG Pola-Ribiere Conjugate Gradient

PTC Parabolic Trough Collector

PTSTPP Parabolic Trough Solar Thermal Power Plant

SCG Scaled Conjugate Gradient

SEA Stirling engine array

SNL Sandia National Laboratory

SPC Solar parabolic concentrator

SRC Steam Rankine Cycle

Greek Symbols

γ_H space ratio in process 12

γ_L space ratio in process 34

μ dynamic viscosity ($\mathrm{kg \cdot m^{-1} \cdot s^{-1}}$)

Subscripts

c cooling fluid

cw cooler wall

h heating fluid

hw heater wall

i inlet

o outlet

p piston

r regenerator

se Stirling engine

th theoretical

Superscripts

$'$ Separate system

List of Figures

Figure 1-1 Alpha-Trough-350, a parabolic trough product made by Alpha-E . 2

Figure 3-1 New arrangement of dish-Stirling system 12
Figure 3-2 5 basic connection types of SEA 16
Figure 3-3 An instance of connection type of an SEA 17
Figure 3-4 T-s diagram of a Stirling cycle 18
Figure 3-5 Flowcharts of the SEA model for performance analysis of the SEAs 28
Figure 3-6 Influence of $T_{i,h}$ on efficiency and power of SEA 30
Figure 3-7 Influence of $q_{m,h}c_{p,h}$ on efficiency and power of SEA 32
Figure 3-8 Influence of $q_{m,c}c_{p,c}$ on efficiency and power of SEA 33
Figure 3-9 Influence of n_{se} on efficiency and power of SEA 34

List of Tables

Table 3.1 Parameters of SEA models 11
Table 3.2 Design specifications of the GPU-3 Stirling engine[1,2] 23
Table 3.3 Thermal efficiency of the proposed Stirling engine model, previous thermal models and experimental data (at $T_{hw} = 922\,\mathrm{K}$ and $T_{cw} = 288\,\mathrm{K}$) 24
Table 3.4 Output power of the proposed Stirling engine model, previous thermal models and experimental data (at $T_{hw} = 922\,\mathrm{K}$ and $T_{cw} = 288\,\mathrm{K}$) 25
Table 3.5 Parameters of SEA models 27
Table 3.6 Results of SEA models under specified parameters 29

Chapter 1 Introduction

> Saving our planet, lifting people out of poverty, advancing economic growth... these are one and the same fight. We must connect the dots between climate change, water scarcity, energy shortages, global health, food security and women's empowerment. Solutions to one problem must be solutions for all.
>
> *Ban Ki-moon*

This dissertation considers a way to solve the global problems of energy shortage and environment problem.

1.1 Solar Parabolic Trough

Parabolic trough solar technology is the most proven and lowest cost large-scale solar power technology available.[3]

Figure 1-1 shows a parabolic trough product made by Alpha-E.

Padilla[4] performed a detailed one dimensional numerical heat transfer analysis of a PTC (Parabolic Trough Collector). To solve the mathematical model of heat transfer of the PTC model, the partial differential equations were discretized and the nonlinear algebraic equations were solved simultaneously. The numerical results was validated to the data from Sandia National Laboratory (SNL).

To understand the thermal performance of the collector and identify the heat losses from the collector, Mohamad[5] analyzed the temperature variation of the working fluid, tube and glass along the collector.

Guo[6] investigated the energy efficiency and exergy efficiency of the parabolic trough collector. The result shown that there exists an optimal mass flow rate of working fluid for

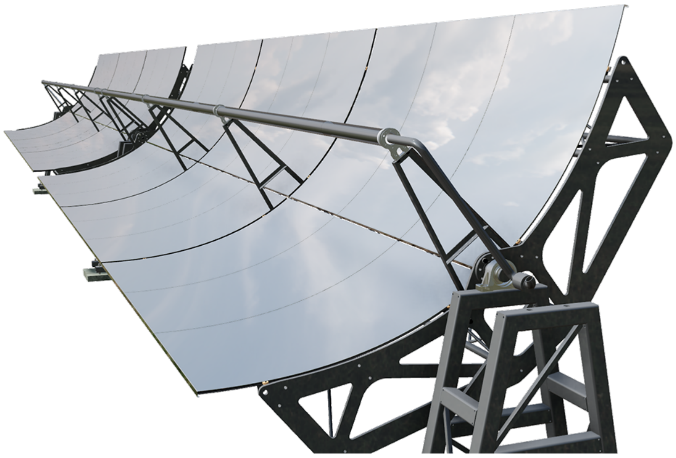

Figure 1-1 Alpha-Trough-350, a parabolic trough product made by Alpha-E

exergy efficiency, and the thermal efficiency and exergy efficiency have opposite changing tendencies under some conditions.

Guo[7] implemented a multi-parameter optimization of parabolic trough solar receiver based on genetic algorithm where Exergy and thermal efficiencies were employed as objective function.

Padilla[8] performed a comprehensive exergy balance of a parabolic trough collector based on the previous heat transfer model[4]. The results shown that inlet temperature of heat transfer fluid, solar irradiance, and vacuum in annulus have a significant effect on the thermal and exergetic performance, but the effect of wind speed and mass flow rate of heat transfer fluid is negligible. It was obtained that inlet temperature of heat transfer fluid cannot be optimized to achieve simultaneously maximum thermal and exergetic efficiency because they exhibit opposite trends. Finally, it was found that the highest exergy destruction is due to the heat transfer between the sun and the absorber while for exergy losses is due to optical error.

Huang[9] proposed an analytical model for optical performance which employed a modified integration algorithm.

Wang[10] proposed a mathematical model for the optical efficiency of the parabolic trough solar collector and selected three typical regions of solar thermal utilization in China for the model. The model is validated by comparing the test results in parabolic trough power plant, with relative error range of 1% to about 5%.

Al-Sulaiman[11] presented the exergy analysis of selected thermal power systems driven by PTSCs. The power pf the thermal power system is produced using either a steam Rankine cycle (SRC) or a combined cycle, in which the SRC is the topping cycle and an organic Rankine cycle (ORC) is the bottoming cycle.

Hachicha[12] presented a detailed numerical heat transfer model based on the finite volume method for the parabolic trough collector. This model is based on finite volume method and ray trace techniques and takes into account the finite size of the Sun. The model is thoroughly validated with results from the literature and it shows a good agreement with experimental and analytical results.

Ashouri[13] coupled a small scale parabolic trough collector and a thermal storage tank along with an auxiliary heater to a Kalina cycle to study the performance of the system throughout the year, both thermodynamically and economically.

Guo[14] developed a nonlinear distribution parameter model to model the dynamic behaviors of direct steam generation parabolic trough collector loops under either full or partial solar irradiance disturbance.

Bader[15] developed a numerical model of a tubular vavity-receiver that uses air as the heat transfer fluid. Four different receiver configurations are considered, with smooth or V-corrugated absorber tube and single- or double-glazed aperture window. The different types of energy loss by the collector have been quantified, and the temperature distribution inside the receiver has been studied. The pumping power required to pump the HTF through the receiver has been determined for a 200 m long collector row.

Good[16] proposed solar trough concentrators using air as heat transfer fluid at operating temperatures exceeding $600\,^{\circ}\mathrm{C}$. It consists of an array of helically coiled absorber tubes contained side-by-side within an insulated groove having a rectangular windowed opening. Secondary concentrating optics are incorporated to boost the geometric concentration ratio to $97\times$.

Boukelia[17] investigated the feed-forward back-propagation learning algorithm with three different variants; Levenberge Marguardt (LM), Scaled Conjugate Gradient (SCG), and Pola-Ribiere Conjugate Gradient (PCG), used in artificial neural network (ANN) to find the best approach for prediction and techno-economic optimization of parabolic trough solar thermal power plant (PTSTPP) integrated with fuel backup system and thermal energy storage.

Kaloudis[18] investigated a PTC system with nanofluid as the HTF in terms of Computational Fluid Dynamics (CFD). Syltherm 800 liquid oil was used as the HTF, and Al_2O_3 nanoparticles with the concentrations ranges from 0% to 4% was investigated. A boost up to 10% on the collector efficiency was reported for Al_2O_3 concentration of 4%.

Tan[19] proposed a two-stage photovoltaic thermal system based on solar trough concentration is proposed, in which the metal cavity heating stage is added on the basis of the PV/T stage, and thermal energy with higher temperature is output while electric energy is output. The experimental platform of the two-stage photovoltaic thermal system was established, with a 1.8 m^2 mirror PV/T stage and a 15 m^2 mirror heating stage, or a 1.8 m^2 mirror PV/T stage and a 30 m^2 mirror heating stage. The results showed that with single cycle, the long metal cavity heating stage would bring lower thermal efficiency, but temperature rise of the working medium is higher, up to 12.06°C with only single cycle. With 30 min closed multiple cycles, the temperature of the working medium in the water tank was 62.8°C, with an increase of 28.7°C, and thermal energy with higher temperature could be output.

Al-Sulaiman[20] proposed a novel system based on PTC and ORC for combined cooling, heating and power (CCHP). Performance assessment, including efficiency, net electrical power, and electrical to heating and cooling ratios, of the system shown that when CCHP is used, the efficiency increases significantly. This study reveals that the maximum electrical efficiency for the solar mode is 15%, for the solar and storage mode is 7%, and for the storage mode is 6.5%. The maximum CCHP efficiency for the solar mode is 94%, for the solar and storage mode is 47%, and for the storage mode is 42%.

Lobon[21] introduced a computational fluid dynamic simulation approach to predict the behavior of a solar steam generating system, which is located at the Plataforma Solar de Almeria, Spain. The CFD package STAR-CCM+ code has been used to implement an efficient multiphase model capable of simulating the dynamics of the multiphase fluid in parabolic-trough solar collectors. Numerical and experimental data are compared in a wide range of working conditions.

Xu[22] presented a method to compensate the end loss effect of PTC. An optical analysis on the end loss effect of PTC with horizontal north-south axis (PTC-HNSA) is performed and a five-meter PTC-HNSA experimental system was built. The increased thermal efficiency of the experimental system is measured, and the result that the experimental value (increased thermal efficiency) substantially agreed with the theoretical value (increased optical efficiency) is gained.

Liu[23] developed a mathematical model of PTC using the least squares support vector machine (LSSVM) method. Numerical simulations are implemented to evaluate the feasibility and efficiency of the LSSVM method, where the sample data derived from the experiment and the simulation results of two solar collector systems with 30 m^2 and 600 m^2 solar fields, and the complicated relationship between the solar collector efficiency and the solar flux, the flow rate and the inlet temperature of the heat transfer fluid (HTF) is extracted.

1.2 Solar Parabolic dish

One of the main goals of the BIOSTIRLING-4SKA project, funded by the European Commission, is the development of a hybrid Dish-Stirling system based on a hybrid solar-gas receiver, which has been designed by the Swedish company Cleanergy.[24]

Craig[25] proposed two types of cooking sections of the solar parabolic dish system: the spiral hot plate copper tube and the heat pipe plate. A conical cavity of copper tubes were put on the focus of the collectors to collect heat and the heat is stored inside an insulated tank which acts both as storage and cooking plate. The use of heat pipes to transfer heat between the oil storage and the cooking pot was compared to the use of a direct natural syphon principle which is achieved using copper tubes in spiral form like electric stove. An accurate theoretical analysis for the heat pipe cooker was achieved by solving the boiling and vaporization in the evaporator side and then balancing it with the condensation and liquid-vapour interaction in the condenser part while correct heat transfer, pressure and height balancing was calculated in the second experiment. The results show and compare the cooking time, boiling characteristics, overall utilization efficiencies and necessary comparison between the two system and other existing systems.

Flux distribution of the receiver is simulated successfully by Mao[26] using MCRT method. The impacts of incident solar irradiation, aspect ratio (the ratio of the receiver height to the receiver diameter), and system error on the radiation flux of the receiver are investigated.

Mawire[27] investigated the thermal performance of a cylindrical cavity receiver for an SK-14 parabolic dish concentrator. The receiver exergy rates and efficiencies are found to be appreciably smaller than the receiver energy rates and efficiencies. The exergy factor is found to be high under conditions of high solar radiation and under high operating temperatures. An optical efficiency of around 52% for parabolic dish system is determined under high solar radiation conditions.

Reddy[28,29] performed the theoretical thermal performance analysis of a fuzzy focal solar parabolic dish concentrator with modified cavity receiver. Total heat loss from the modified cavity receiver is estimated considering the effects of wind conditions, operating temperature, emissivity of the cavity cover and thickness of insulation. Time constant test was carried out to determine the influence of sudden change in solar radiation at steady state conditions. The daily performance tests were conducted for different flow rates.

Vikram[30] investigated the total heat losses of modified cavity receiver of SPD with three configurations using 3D numerical model. The effects of various parameters such as diameter ratio, angle of inclination, operating temperature, insulation thickness and emissivity of the cavity cover on the heat losses from the modified vavity receiver are investigated. An ANN model is developed to predict the heat loss for a large set of influencing parameters. Based on ANN modeling, improved Nusselt number correlations are proposed for convective, radiative and total heat losses from the modified cavity receiver. The convective heat losses are greatly influenced by receiver inclination whereas the radiation heat losses are influenced by the cavity cover emissivity. The diameter ratio also plays a major role in heat losses from the cavity receiver. The present method predicts the heat losses more accurately compared with the existing models.

Atul[31] proposed a low-cost solar dish water heating system and investigated the effect of variation of mass flow rate on performance of the heater prototype. A novel truncated cone-shaped helical coiled receiver made up of copper is put at the focal point of SP.

CRTEn developed a solar parabolic concentrator (SPC) using four types of absorbers: flat plat, disk, water calorimeter and solar heat exchanger.[32] For the system different types of absorbers, experiments were conducted to obtain the mean concentration ratio and both energy and exergy efficiency. Results shown that thermal energy efficiency of the system varies from 40% to 77%, the concentrating system reaches an average exergy efficiency of 50% and a concentration factor around 178.

Blazquez[24] studied the optimization of the concentrator and receiver cavity geometry of parabolic dish system. Ray-tracing analysis has been performed with the open source software Tonatiuh, a ray-tracing tool specifically oriented to the modeling of solar concentrators.

Uma[33] carried out the simulation of the structural, thermal and CFD analysis of the dish with varying metallic properties (Aluminium, Copper and StainlessSteel) under different wind conditions. Computational Fluid Dynamics (CFD) was done to simulate the thermal performance of the dish at two different wind velocities.

Patil[34] described the development of automatic dual axis solar tracking system for solar parabolic dish. Five light dependent resistors were used to sense the sunlight and Two permanent magnet DC motors are used to move the solar dish. A controller software were developed to control the motors using the data sensed by the resistors.

Pavlovic[35] presented a procedure to design a square facet concentrator for laboratory-scale research on medium-temperature thermal processes. A parabolic collector made up of individual square mirror panels (facets) were investigated. These facets can deliver up to 13.604 kW radiative power over a 250 mm radius disk (receiver) with average concentrating ratio exceeding 1200.

1.3 Solar Tower

Solar tower

1.4 Rankine Cycle

1.5 Stirling Engine

A large number of studies have been done on Stirling engine analysis. To describe a Stirling engine's behavior precisely is a difficult task due to the various losses and irreversibilities in the engine. Researchers have done a lot of work to build a precise Stirling engine model. Different models of Stirling engines were developed using empirical[36–41], analytical[42–51] and numerical methods[1,52–61].

Among these methods, numerical methods obtain the most accurate models. Urieli and Berchowitz[52] proposed an adiabatic model of Stirling engine considering some irreversible effects such as non-ideal heat transfer processes and pressure drop effect using numerical methods. The model is known as Simple model. Many researchers developed more accurate models based on the Simple model by using alternative methods or including more loss mechanisms. Ni et al.[53] proposed an improved Simple analytical model which considers the influence mechanism of rotary speed, pressure and working gas in the view of heat/power losses for Stirling engine performance. Jia et al.[54] developed a numerical model of free-piston engine generator. The dynamic equations have been linearized to simplify the model to a one-degree forced vibration system with various damping. The solving time of the proposed fast response model can be significantly reduced comparing to previous numerical models. Strauss and Dobson[55] proposed an alternative method to calculate the regeneration heat loss and pumping losses, which is more suitable for preliminary engine design and optimisation, known as Simple II model. Abbas[56] considered the effects of non-ideal regeneration, shuttle loss and heat conduction losses based on Simple model. Araoz et al.[57] developed a rigorous Stirling engine model with adiabatic working spaces, isothermal heat exchangers. It considers dead volumes, and imperfect regeneration, mechanical pumping losses due to friction, limited heat transfer and thermal losses on the heat exchangers. The model is suitable for different engine configurations (α, β and γ engines). Babaelahi and Syyaadi[1] proposed a new numerical thermal model based on polytropic expansion/-compression processes. Differential equations in the expansion/compression processes were modified to polytropic processes in the new model. New model shows a better performance prediction compared with previous models.

With the development of finite-time thermodynamics, many researchers studied the the finite-time thermodynamic performance of the Stirling engine. This analysis can also be used in the case of irreversible machines further considering the internal irreversibilities of a Stirling engine such as friction, pressure drop and entropy generation[58]. Wu et al.[59] developed a numerical model considering finite-time effect to find out the relationship between the net power output and thermal efficiency of the engine. Li et al.[60] developed a mathematical model of a high temperature differential dish-Stirling system with finite-time thermodynamics. Finite-rate heat transfer, regenerative heat losses, conductive thermal bridging losses and finite regeneration processes of the Stirling engine were considered in the model. Hosseinzade[61] presented a new closed-form thermal model for the thermal simulation of Stirling engines based on the combination of polytropic analysis of expansion/compression processes and the concept of finite speed thermodynamics. Instead of finite-time method, Ahmadi et al.[62] proposed a finite-speed thermodynamic analysis based on the first law of thermodynamics for a closed system with finite speed and the direct method. The effects of heat source temperature, regenerating effectiveness, volumetric ratio, piston stroke as well as rotational speed are included in the analysis. Chen et al.[63] developed a heat-engine cycle model using finite-time thermodynamics. The model, considered the losses due to heat-resistance, heat leaks and internal irreversibility, is applicable for generalized irreversible universal steady-flow heat-engine cycles.

On the other side of the researches, multi-objective optimization algorithms were used considering multi-variables to obtain a better performance was paid for attention by numbers of researchers recently[64–67]. Ahmadi et al.[64] performed the thermodynamic analysis of solar dish Stirling engine based on the finite-time thermodynamics. Then the NSGA-II algorithm was applied. Three objectives, thermal efficiency, entransy loss rate and power output, were set as the objectives and three well known decision making methods have been employed in the algorithm. Li et al.[65] developed a multi-objective optimization model of a solar energy powered gamma type Stirling engine using Finite Physical Dimensions Thermodynamics (FPDT) method by multi-objective criteria. Genetic algorithm was used to get the Pareto frontier, and optimum points were obtained using the decision different making methods. Results show that total thermal conductance, hot temperature, stroke and diameter ratios can be improved. Patel and Savsani[66] developed a strategy for multi-objective optimization for Stirling engines using TS-TLBO (tutorial training and self learning inspired teaching-learning-based optimization) algorithm. An application example with eleven decision variables and three objectives are considered. Luo et al.[67] proposed a multiple optimization method that combines multiple optimization algorithms including differential evolution, genetic algorithm and adaptive simulated annealing. The optimization considers five decision variables, including engine frequency, mean effective pressure, temperature of heating source, number of wires in regenerator matrix, and the wire diameter of regenerator for maximum efficiency and output power.

1.6 Brayton Cycle

1.7 Research Objective

Chapter 2 System Design

2.1 System Structure

2.2 Component Modeling

Object oriented method is used for system modeling.

2.2.1 Solar Parabolic Trough

2.2.2 Solar Parabolic Dish

2.2.2.1 Solar Dish Collector

2.2.2.2 Solar Dish Receiver

2.2.3 Steam Generators

2.2.4 Power Block

2.2.5 Condenser

2.2.6 Deareator

2.2.7 Stirling Engine

2.2.8 Heat Storage System

Chapter 3 System Analysis

3.1 Energy Cascade Collection

3.2 Energy Cascade Utilization

Table 3.1 Parameters of SEA models

Parameters	Value
s_{se}	20 Hz
$U_h A_h$	180 W/K
$U_c A_c$	180 W/K
n_{se}	6
$q_{m,h}$	0.3 kg/s
$q_{m,c}$	0.3 kg/s
$P_{i,h}$	5×10^5 Pa
$P_{i,c}$	5×10^5 Pa

3.3 Stirling Engine Array

3.4 Introduction

With the emphasis on energy and environmental impact, recently gaining attention is focused on Stirling engine for its high efficiency, low maintenance requirement, flexibility on energy sources, no pollution, low explosion risk. Due to its closed cycle, it can use almost any heat source, which makes it compatible with alternative and renewable energy sources.

The Stirling engine is widely used on solar dish system, known as dish-Stirling system. In a traditional dish-Stirling system, each Stirling engines is put on the focus of a parabolic dish to use the heat collected by the dish receiver for power generation. However, solar dish systems are not widely applied yet for its small capacity. Its capacity is mainly constrained by two factors: dish collector size and Stirling engine size. The dish size is limited for the cost and difficulty of production of large mirrors. The Stirling engine size is limited for its low power-to-weight ratio. The tracking feature of dish collector limits the weight of engine on the focal point. Besides, the size of engine is limited for it overlaps part of the collector.

This paper presents new arrangements for dish-Stirling system demonstrated in Figure 3-1 to solve the limitations. Stirling engines are put on the ground as a Stirling engine array (SEA). Heat collected by multiple dish collectors, or other types of collectors, or combination of different types of collectors, even heat from different heat sources is supplied to the SEA. Since the engines are static installations on the ground where space and weight are not at a premium any more, they can reach higher capacities. They can be connected in a different connection type and their performance may be improved compared to the traditional arrangement in which they are put on the focal points of each dish collector separately.

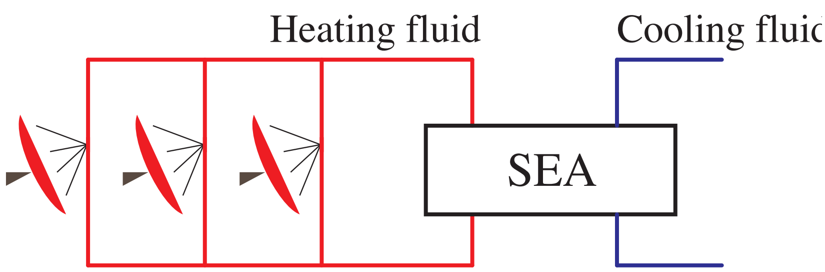

Figure 3-1 New arrangement of dish-Stirling system

Great attention has focused on the application using parabolic dish to collect heat. Some researchers investigated the impact of various parameters on the optical and thermal performance of the solar dish receivers using Monte Carlo Ray Tracing Method (MCRTM) and/or numerical modeling methods[68–74]. Some researchers considered the applications with different ways to use the collected heat. Loni et al.[75] considered a system using parabolic dish for an organic Rankine cycle. In the proposed system, thermal oil is used as the working fluid to transport the collected heat for the organic Rankine cycle. Wang et al.[76] proposed an inverse design method for a cavity receiver used in solar dish Brayton system. Craig et al.[77] evaluated a parabolic dish tubular receiver used in a dish Brayton cycle. An approach for incorporating a complex geometry like a tubular receiver generated using CFD software into SolTrace was developed. Aichmayer et al.[78] presented a hybrid solar micro gas-turbine system integrating volumetric solar dish receiver. Concerning the solar dish receiver integration, both pressurized and atmospheric configurations have been considered. Lovegrove et al.[79] presented an idea of using parabolic dish array to provide heat for ammonia based thermochemical energy storage. In this regard, using parabolic dishes to provide heat for SEA is applicable.

A large number of studies have been done on Stirling engine analysis. To describe a Stirling engine's behavior precisely is a difficult task due to the various losses and irreversibilities in the engine. Researchers have done a lot of work to build a precise Stirling engine model. Different models of Stirling engines were developed using empirical[36–41], analytical[42–51] and numerical methods[1,52–61].

Among these methods, numerical methods obtain the most accurate models. Urieli and Berchowitz[52] proposed an adiabatic model of Stirling engine considering some irreversible effects such as non-ideal heat transfer processes and pressure drop effect using numerical methods. The model is known as Simple model. Many researchers developed more accurate models based on the Simple model by using alternative methods or including more loss mechanisms. Ni et al.[53] proposed an improved Simple analytical model which considers the influence mechanism of rotary speed, pressure and working gas in the view of heat/power losses for Stirling engine performance. Jia et al.[54] developed a numerical model of free-piston engine generator. The dynamic equations have been linearized to simplify the model to a one-degree forced vibration system with various damping. The solving time of the proposed fast response model can be significantly reduced comparing to previous numerical models. Strauss and Dobson[55] proposed an alternative method to calculate the regeneration heat loss and pumping losses, which is more suitable for preliminary engine design and optimisation, known as Simple II model. Abbas[56] considered the effects of non-ideal regeneration, shuttle loss and heat conduction losses based on Simple model. Araoz et al.[57] developed a rigorous Stirling engine model with adiabatic working spaces, isothermal heat exchangers. It considers dead volumes, and imperfect regeneration, mechanical pumping losses due to friction, limited heat transfer and thermal losses on the heat exchangers. The model is suitable for different engine configurations (α, β and γ engines). Babaelahi and Syyaadi[1] proposed a new numerical thermal model based on polytropic expansion/-compression processes. Differential equations in the expansion/compression processes were modified to polytropic processes in the new model. New model shows a better performance prediction compared with previous models.

With the development of finite-time thermodynamics, many researchers studied the the finite-time thermodynamic performance of the Stirling engine. This analysis can also be used in the case of irreversible machines further considering the internal irreversibilities of a Stirling engine such as friction, pressure drop and entropy generation[58]. Wu et al.[59] developed a numerical model considering finite-time effect to find out the relationship between the net power output and thermal efficiency of the engine. Li et al.[60] developed a mathematical model of a high temperature differential dish-Stirling system with finite-time thermodynamics. Finite-rate heat transfer, regenerative heat losses, conductive thermal bridging losses and finite regeneration processes of the Stirling engine were considered in the model. Hosseinzade[61] presented a new closed-form thermal model for the thermal simulation of Stirling engines based on the combination of polytropic analysis of expansion/compression processes and the concept of finite speed thermodynamics. Instead of finite-time method, Ahmadi et al.[62] proposed a finite-speed thermodynamic analysis based on the first law of thermodynamics for a closed system with finite speed and the direct method. The effects of heat source temperature, regenerating effectiveness, volumetric ratio, piston stroke as well as rotational speed are included in the analysis. Chen et al.[63] developed a heat-engine cycle model using finite-time thermodynamics. The model, considered the losses due to heat-resistance, heat leaks and internal irreversibility, is applicable for generalized irreversible universal steady-flow heat-engine cycles.

On the other side of the researches, multi-objective optimization algorithms were used considering multi-variables to obtain a better performance was paid for attention by numbers of researchers recently[64–67]. Ahmadi et al.[64] performed the thermodynamic analysis of solar dish Stirling engine based on the finite-time thermodynamics. Then the NSGA-II algorithm was applied. Three objectives, thermal efficiency, entransy loss rate and power output, were set as the objectives and three well known decision making methods have been employed in the algorithm. Li et al.[65] developed a multi-objective optimization model of a solar energy powered gamma type Stirling engine using Finite Physical Dimensions Thermodynamics (FPDT) method by multi-objective criteria. Genetic algorithm was used to get the Pareto frontier, and optimum points were obtained using the decision different making methods. Results show that total thermal conductance, hot temperature, stroke and diameter ratios can be improved. Patel and Savsani[66] developed a strategy for multi-objective optimization for Stirling engines using TS-TLBO (tutorial training and self learning inspired teaching-learning-based optimization) algorithm. An application example with eleven decision variables and three objectives are considered. Luo et al.[67] proposed a multiple optimization method that combines multiple optimization algorithms including differential evolution, genetic algorithm and adaptive simulated annealing. The optimization considers five decision variables, including engine frequency, mean effective pressure, temperature of heating source, number of wires in regenerator matrix, and the wire diameter of regenerator for maximum efficiency and output power.

However, the literature review indicates that the analysis of arrangements of Stirling engines, classification and performance of the SEA, has not been reported till now. In this regard, this paper investigated the connection types of SEA and its influence on SEA performance. Connection types of SEA were classified and 5 basic connection types were put forward. According to Organ's theory[80], one equivalent analytical Stirling engine model always exists for different types (α type, β type and γ type) of engines. To find out the influence of connection type of SEA and to avoid falling into the problem of developing specific Stirling engine model, a Stirling engine model based on some assumptions and simplifications was developed. This model was evaluated using experimental data of the General Motor GPU-3 Stirling engine prototype. Imperfect regeneration and some irreversibilities were considered. Heat transfer analysis of Stirling engine with heating and cooling fluids was also included. SEA models of different connection types were built depending on the engine model. Impacts of different parameters on the performance of these models were analyzed.

3.5 Connection types of SEA

For a single Stirling engine, the heat transfer processes between fluids and engine are independent and irrelevant with the direction of the flows, which means the efficiency and power are not affected by the direction of fluids. However, for an SEA, the connection type will affect the temperature profiles through the array and the specific work production, both of which will determine the efficiency and power of the SEA. It is practically significant to investigate the influence of connection type of an SEA on its performance. Then it is essential to classify the SEAs based on the connection type.

5 basic connection types of SEA were summarized according to the direction-irrelevant feature of Stirling engine, as shown in Figure 3-2. Type 1 is parallel flow, Type 2 is serial flows in the same order, Type 3 is serial flows in the reverse order, Type 4 is heating fluid in serial flow and cooling fluid in parallel flow and Type 5 is heating fluid in parallel flow and cooling fluid in serial flow.

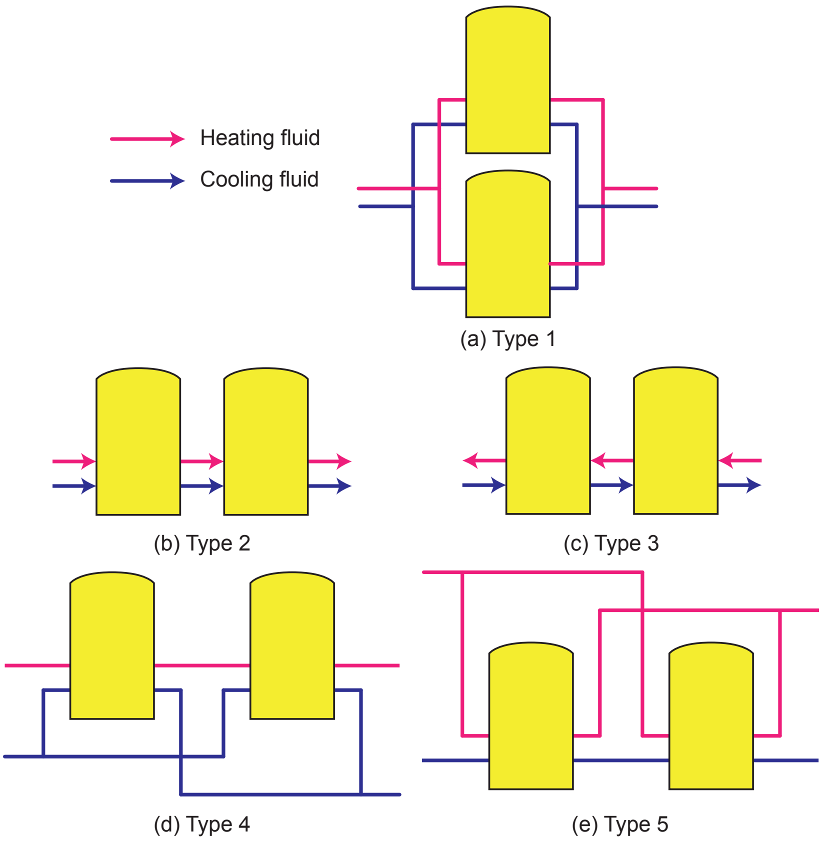

Figure 3-2 5 basic connection types of SEA

All other connection types are the combination of these 5 basic connection types. For instance, an SEA in Figure 3-3 is the combination of Type 2 and Type 4.

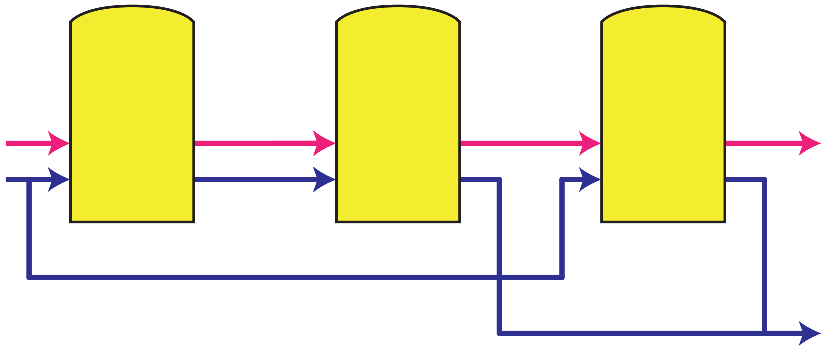

Figure 3-3 An instance of connection type of an SEA

3.6 Thermodynamic analysis of Stirling engine

3.6.1 Stirling engine model

3.6.1.1 Theoretical Stirling cycle

In a Stirling cycle, there are two isothermal processes that exchange heat with heating and cooling fluids, two isochoric processes that exchange heat with regenerator. In Figure 3-4, the heat absorbed by regenerator in process 4-1 is reused in process 2-3, but only able to heat the working gas from 2 to 3' due to the imperfect regeneration. e is defined as the regenerator effectiveness[46,81], $e = \frac{T_R - T_L}{T_H - T_L}$, where T_H is the temperature in the hot space, T_L is the temperature in the cold space, T_R is the effective working fluid temperature in the regenerator.

In order to obtain a simplified analytical model, several simplifications were made:

- The working gas in Stirling engines obeys the idea gas law.
- No heat loss to the environment for Stirling engines.
- Overall heat transfer coefficients of the fluids are constant.
- A symmetrical regenerator behavior is assumed[46,81] so that a simple effectiveness can be obtain by $T_R = \frac{T_H - T_L}{\ln(T_H/T_L)}$.

To consider internal irreversibilities in Stirling cycle made by dead volumes, as described in[82], total dead volume V_D is divided into heater dead volume V_{DH}, regenerator dead volume V_{DR} and cooler dead volume V_{DC}. There exists a factor K to describe the dead

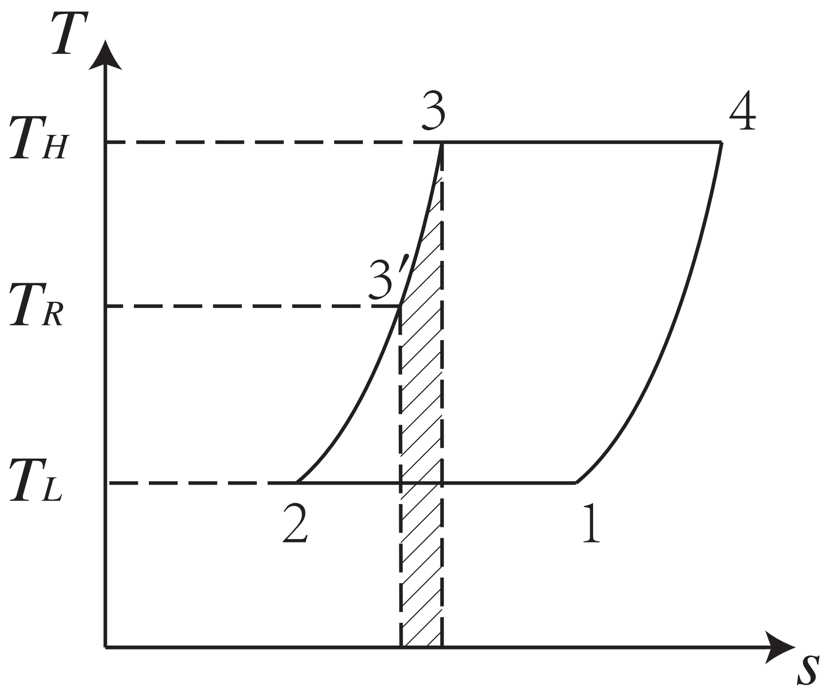

Figure 3-4 T-s diagram of a Stirling cycle

volumes under different temperatures. K is relevant with temperatures in the process and regenerator effectiveness.

$$K = \frac{V_{DH}}{T_H} + \frac{V_{DR}}{T_R} + \frac{V_{DC}}{T_L} \tag{3.1}$$

For the isothermal compression process 1-2, the output work

$$W_{12} = \int_{V_E+V_C}^{V_E} p_{12} dV = -mRT_L \ln \frac{V_E + V_C + KT_L}{V_E + KT_L} \tag{3.2}$$

For the isothermal expansion process 3-4, the output work

$$W_{34} = \int_{V_E}^{V_E+V_C} p_{34} dV = mRT_H \ln \frac{V_E + V_C + KT_H}{V_E + KT_H} \tag{3.3}$$

Define $\gamma_H = \frac{V_E+V_C+KT_H}{V_E+KT_H}$, and $\gamma_L = \frac{V_E+V_C+KT_L}{V_E+KT_L}$, so in a cycle, the theoretical output work

$$W_{th} = W_{12} + W_{34} = mR(T_H \ln \gamma_H - T_L \ln \gamma_L) \tag{3.4}$$

For the isochoric heating process 3'-3, the absorbed heat

$$Q_{3'3} = nc_v(T_H - T_R) = \frac{1-e}{k-1} mR(T_H - T_L) \tag{3.6}$$

For the the isothermal expansion process 3-4, the absorbed heat

$$Q_{34} = W_{34} = mRT_H \ln \gamma_H \tag{3.7}$$

In a cycle, the theoretical absorbed heat

$$Q_{th} = Q_{3'3} + Q_{34} = \frac{1-e}{k-1} mR(T_H - T_L) + mRT_H \ln \gamma_H \tag{3.8}$$

3.6.1.2 Irrevisibilities and losses

1. Non-ideal heat transfer effect
   Because of non-ideal heater and cooler, the working fluid temperature (T_H/T_L) in these two heat exchangers is less/higher than the wall temperature (T_{hw}/T_{cw}), respectively. And T_H and T_L can be corrected by the wall temperatures as follows:

$$T_H = T_{hw} - \frac{Qs_{se}}{h_h A_{hw}} \tag{3.9}$$

$$T_L = T_{cw} + \frac{(Q-W)s_{se}}{h_c A_{cw}} \tag{3.10}$$

The heat transfer coefficient can be obtained using the following correlation[1]:

$$h_{h,c} = \frac{\mu c_p f_{Re}}{2D_{h,c} Pr_{h,c}} \tag{3.11}$$

where f_{Re} is a Reynolds friction factor defined as:

$$f_{Re} = 0.0791 {Re_{h,c}}^{0.75} \tag{3.12}$$

$Re_{h,c}$, $Pr_{h,c}$ and $D_{h,c}$ are Reynolds number, Prandtl number and hydraulic diameter of the heater/cooler exchanger.

2. Effect of pressure drop

   Pressure drops in the heat exchangers cause power losses of the Stirling engine. The pressure drops can be obtained by[52]:

$$\Delta p = -\frac{2 f_{Re} \mu u V}{d^2 A} \tag{3.13}$$

   where u is the working gas speed, V is volume, A is flow cross-section area.

   The net power loss of the Stirling engine due to pressure drop of the heat exchangers can be evaluated by:

$$W_{pd} = \oint \sum_{i=E,C} (\Delta p_i \frac{dV_i}{d\theta}) d\theta \tag{3.14}$$

3. Effect of finite speed of piston and mechanical friction

   Due to the finite speed of piston, the pressure on the piston surface is different from the pressure of expansion and compression spaces. It has been demonstrated that the pressure on the piston surface in the expansion process is less than the mean pressure in the expansion space. Similarly, the pressure on the piston surface in the compression process is greater than the mean pressure in the compression space. This means the output work is less than the theoretical value. Besides, The output work also reduces due to mechanical friction. The output work loss due to finite speed of piston and mechanical friction can be obtained as follows[1]:

$$W_{fs} = \oint p(\pm \frac{a u_p}{c} \pm \frac{\Delta p_f}{p}) dV \tag{3.15}$$

   where the sign (+) is used in the compression space, and the sign (-) is used in the expansion space. p is the mean pressure in the compression/expansion space, u_p is velocity of the piston, c is the average speed of molecules and Δp_f is the pressure loss due to mechanical friction. Δp_f, a and c can be obtained by[83]:

$$\Delta p_f = 0.97 + 0.009 s_{se} \tag{3.16}$$

$$a = \sqrt{3k} \tag{3.17}$$

$$c = \sqrt{3RT} \tag{3.18}$$

4. Energy losses due to internal conduction

   The temperature differs from the heater and cooler, heat losses from heater to cooler exists due to internal conduction through the walls of regenerator.[55] The internal conduction loss in a cycle can be obtained by follows:

$$Q_{id} = \frac{k_r A_r}{L_r s_{se}}(T_{hw} - T_{cw}) \tag{3.19}$$

   where, k_r, A_r and L_r denote the regenerator matrix conductivity, regenerator length, and regenerator conductive area respectively.

5. Energy losses due to shuttle conduction

   The displacer shuttles between the expansion and compression space. It absorbs heat during the hot end of its stroke and releases it during the cold end of its stroke. This heat loss can be estimated as[84]:

$$Q_{sc} = 0.4\frac{Z^2 k_p D_p}{J L_d s_{se}}(T_H - T_L) \tag{3.20}$$

   where, Z, k_p, D_p, J and L_d denote the displacer stroke, piston thermal conductivity, displacer diameter, gap between the displacer and the cylinder, and length of the displacer respectively.

So, in a Stirling engine, the total absorbed heat in a cycle

$$Q = Q_{th} + Q_{id} + Q_{sc} \tag{3.21}$$

the output work

$$W = W_{th} - W_{pd} - W_{fs} \tag{3.22}$$

Power of the Stirling engine

$$P = Ws_{se} \tag{3.23}$$

Efficiency of the Stirling engine

$$\eta = W/Q \tag{3.24}$$

3.6.2 Model validation

Evaluation of the developed thermal model was performed by considering the GPU-3 Stirling engine as a case study. Design specifications of the GPU-3 Stirling engine are indicated in Table 3.2. The thermal efficiency and power of the proposed Stirling engine model was compared with previous thermal models and experimental data as shown in Table 3.3 and Table 3.4.

It can be found that the proposed model has much better agreement with the experimental results than previous thermal models at various rotation speeds and mean effective pressures. It is required to mention that in all thermal models both power W and input heat Q were determined by the thermal process of heat transfer between the wall and working gas. In the proposed model, W and Q are obtained by Equation 3.9 and 3.10. Therefore all the three parameters W, Q and η are determined by the thermal model and input parameters to the model. These input parameters includes heater, cooler, mean effective pressure, type of working gas and geometrical specification of the engine.

Table 3.3 and 3.4 indicate that when mean effective pressure of the engine increases from 2.76 MPa to 6.90 MPa, best performance (efficiency and power) prediction of the proposed model exists. When rotation speed increases from 16.67 Hz to 58.33 Hz, error in prediction of performance of the proposed model increases. The proposed model may have the best performance prediction at a low rotation speed, with mean effective pressure between 4.14 MPa and 5.52 MPa.

However, there is still some discrepancy between the the simulation results of proposed model and the experimental data. In the future researches, more accurate models of Stirling engine may be developed by considering other irreversibilities such as heat loss to the environment, gas spring hysteresis, and etc. It is worth pointing that there are more accurate Stirling engine models. For example, polytropic simulation models of Stirling engine

Table 3.2 Design specifications of the GPU-3 Stirling engine[1,2]

Parameter	Value
Engine type	β
Working gas	Helium
Mass of the working gas	1.136 g
Heater	
Number of tubes	40
Tube external diameter	4.83×10^{-3} m
Tube internal diameter	3.02×10^{-3} m
Tube length (cylinder side)	0.1164 m
Tube length (regenerator side)	0.1289 m
Cooler	
Number of tubes	312
Tube external diameter	1.59×10^{-3} m
Tube internal diameter	1.09×10^{-3} m
Average tube length	4.61×10^{-2} m
Regenerator	
Number of regenerator	8
Regenerator internal diameter	2.26×10^{-2} m
Regenerator length	2.26×10^{-2} m
Diameter of regenerator tube	4×10^{-5} m
Material	Stainless steel
Volume	
Swept Vol. (expansion/compression)	120.82/114.13 cm^3
Clearance Vol. (expansion/compression)	30.52/28.68 cm^3
Dead Vol. (heater/cooler/regenerator)	70.28/13.18/50.55 cm^3

Table 3.3 Thermal efficiency of the proposed Stirling engine model, previous thermal models and experimental data (at $T_{hw} = 922\,\mathrm{K}$ and $T_{cw} = 288\,\mathrm{K}$)

Rotation speed (Hz)	Mean effective pressure (MPa)	Thermal efficiency predicted by the simple analysis (variable Pr[52]) Value (%)	Error (%)	Average error (%)	Thermal efficiency predicted by the adiabatic analysis (simple II[55]) Value (%)	Error (%)	Average error (%)	Thermal efficiency predicted by the proposed Stirling Engine model Value (%)	Error (%)	Average error (%)	Exper efficie Ac va (%
16.67	2.76	38.72	18.22	17.90	32.48	11.98	12.85	28.16	7.66	12.10	20
25.00		36.16	15.46		31.21	10.51		27.75	7.05		20
33.33		33.79	15.79		29.45	11.45		27.43	9.43		18
41.67		31.48	16.28		27.45	12.25		27.17	11.97		15
50.00		29.12	17.32		25.21	13.41		26.94	15.14		11
58.33		29.74	24.34		22.89	17.49		26.74	21.34		5.
25.00	4.14	35.65	10.85	11.46	32.29	7.49	8.28	27.29	2.49	6.65	24
33.33		33.52	9.62		30.40	6.50		26.94	3.04		23
41.67		31.48	10.18		28.39	7.09		26.65	5.35		21
50.00		29.45	11.25		26.33	8.13		26.39	8.19		18
58.33		27.40	15.40		24.21	12.21		26.17	14.17		12
41.67	5.52	31.20	8.70	10.82	28.59	6.09	8.11	26.24	3.74	7.48	22
50.00		29.33	10.53		26.62	7.82		25.97	7.17		18
58.33		27.44	13.24		24.62	10.42		25.73	11.53		14
50.00	6.90	29.07	10.37	11.73	26.61	7.91	9.19	25.62	6.92	9.05	18
58.33		27.29	13.09		24.67	10.47		25.37	11.17		14

Table 3.4 Output power of the proposed Stirling engine model, previous thermal models and experimental data (at $T_{hw} = 922\,\mathrm{K}$ and $T_{cw} = 288\,\mathrm{K}$)

Rotation speed (Hz)	Mean effective pressure (MPa)	Output power predicted by the simple analysis (variable Pr[52])			Output power predicted by the adiabatic analysis (simple II[55])			Output power predicted by the proposed Stirling Engine model			Ex ou po (k
		Value (kW)	Error (%)	Average error (%)	Value (kW)	Error (%)	Average error (%)	Value (kW)	Error (%)	Average error (%)	
16.67	2.76	1.796	119.02	272.03	1.772	116.10	254.71	0.861	4.98	104.84	
25.00		2.555	128.13		2.500	123.21		1.253	11.88		
33.33		3.215	165.70		3.117	157.60		1.632	34.88		
41.67		3.769	211.49		3.615	198.76		2.001	65.37		
50.00		4.195	303.37		3.973	282.08		2.362	127.12		
58.33		4.505	704.46		4.203	650.54		2.715	384.82		
25.00	4.14	3.844	114.75	259.70	3.761	110.11	158.41	1.818	1.56	39.83	
33.33		4.856	120.73		4.708	114.00		2.362	7.36		
41.67		5.734	136.94		5.501	127.31		2.890	19.42		
50.00		6.462	174.98		6.126	160.68		3.405	44.89		
58.33		7.030	306.36		6.573	279.94		3.908	125.90		
41.67	5.52	7.645	133.08	180.02	7.334	123.60	164.91	3.742	14.09	43.68	
50.00		8.655	163.87		8.206	150.18		4.401	34.18		
58.33		9.470	243.12		8.858	220.94		5.045	82.79		
50.00	6.90	10.788	174.50	287.04	10.223	160.13	263.63	5.362	36.44	97.75	
58.33		11.840	399.58		11.071	367.13		6.140	159.07		

show higher accuracy than our proposed model[1,61]. However, the model needs more costly calculations and the polytropic indexes are engine-specific.

3.6.3 Heat transfer between the engine and the fluids

For a Stirling engine thermal process, the wall temperatures of the heater and cooler are considered to be uniform and constant. The heat transferred between the wall and the fluids is

$$(T_w - T)UdA = q_m c_p dT \tag{3.25}$$

with $T(0) = T_i, T(A) = T_o$,

$$\frac{T_o - T_w}{T_i - T_w} = \exp(-\frac{UA}{q_m c_p}) \tag{3.26}$$

For a Stirling engine, T_{hw} or T_{cw} can be used to substitute T_w to get the relationships between $T_{i,h}$, $T_{o,h}$ and T_{hw}, or $T_{i,c}$, $T_{o,c}$ and T_{cw} respectively.

$$\frac{T_{o,h} - T_{hw}}{T_{i,h} - T_{hw}} = \exp(-\frac{U_h A_h}{q_{m,h} c_{p,h}}) \tag{3.27}$$

$$\frac{T_{o,c} - T_{cw}}{T_{i,c} - T_{cw}} = \exp(-\frac{U_c A_c}{q_{m,c} c_{p,c}}) \tag{3.28}$$

Heat transferred from heating fluid to Stirling engine in a cycle

$$q_{m,h} c_{p,h} (T_{i,h} - T_{o,h})/s_{se} = Q \tag{3.29}$$

Heat transferred from Stirling engine to cooling fluid in a cycle

$$q_{m,c} c_{p,c} (T_{o,c} - T_{i,c})/s_{se} = Q - W \tag{3.30}$$

3.7 Modeling of the SEAs

To determine the performance of an SEA, models of all the Stirling engines need to be built depending on their thermodynamic characteristic. Stirling engines are chosen to have the same parameters including the same speed s_{se}. This is especially practical when using

SEA for power generation, where the output power frequency should be constant. The speed of Stirling engine can be calibrated by speed controller system[85]. To eliminate interference of other factors, heating and cooling fluids are chosen to have same parameters for different connection types of SEAs. To clearly find out the performance differences of different SEAs, large temperature differences of the heating/cooling fluids after heat exchange with the engines are preferred. Air is chosen as the cooling fluid instead of commonly used water to avoid small temperature rise and evaporation after the cooling process. Chosen parameters of Stirling engines and heating/cooling fluids in SEAs are shown in Table 3.5.

Table 3.5 Parameters of SEA models

Parameter	Value	Parameter	Value
Heating fluid	Air	$q_{m,h}$	0.4 kg/s
Cooling fluid	Air	$T_{i,h}$	1000 K
n_{se}	6	$p_{i,h}$	5×10^5 Pa
s_{se}	25 Hz	$q_{m,c}$	0.4 kg/s
p_{se}	5 MPa	$T_{i,c}$	300 K
U_hA_h	180 W/K	$p_{i,c}$	5×10^5 Pa
U_cA_c	180 W/K		

In an SEA, there are 2 flows as shown in Figure 3-2. In a serial flow, each engine's mass flow rate is q_m, and from the flow's direction, for $2 \leqslant x \leqslant n_{se}$, $T_{i,x} = T_{o,x-1}$. In a parallel flow, each engine's mass flow is q_m/n_{se}, for $2 \leqslant x \leqslant n_{se}$, $T_{i,x} = T_{i,h}$.

MATLAB was used as the programming tool to build the model of SEAs, and CoolProp was used to provide fluid properties for MATLAB program. 5 basic SEA models composed of the aforementioned Stirling engines and fluids were built. To compare SEA connection types under various conditions, several parameters are investigated to find out their effects on SEA performance.

Figure 3-5 shows the solution algorithm of the SEA model. As it is shown, known inlet parameters of the fluids, the performance of a Stirling engine can be obtained from flowchart

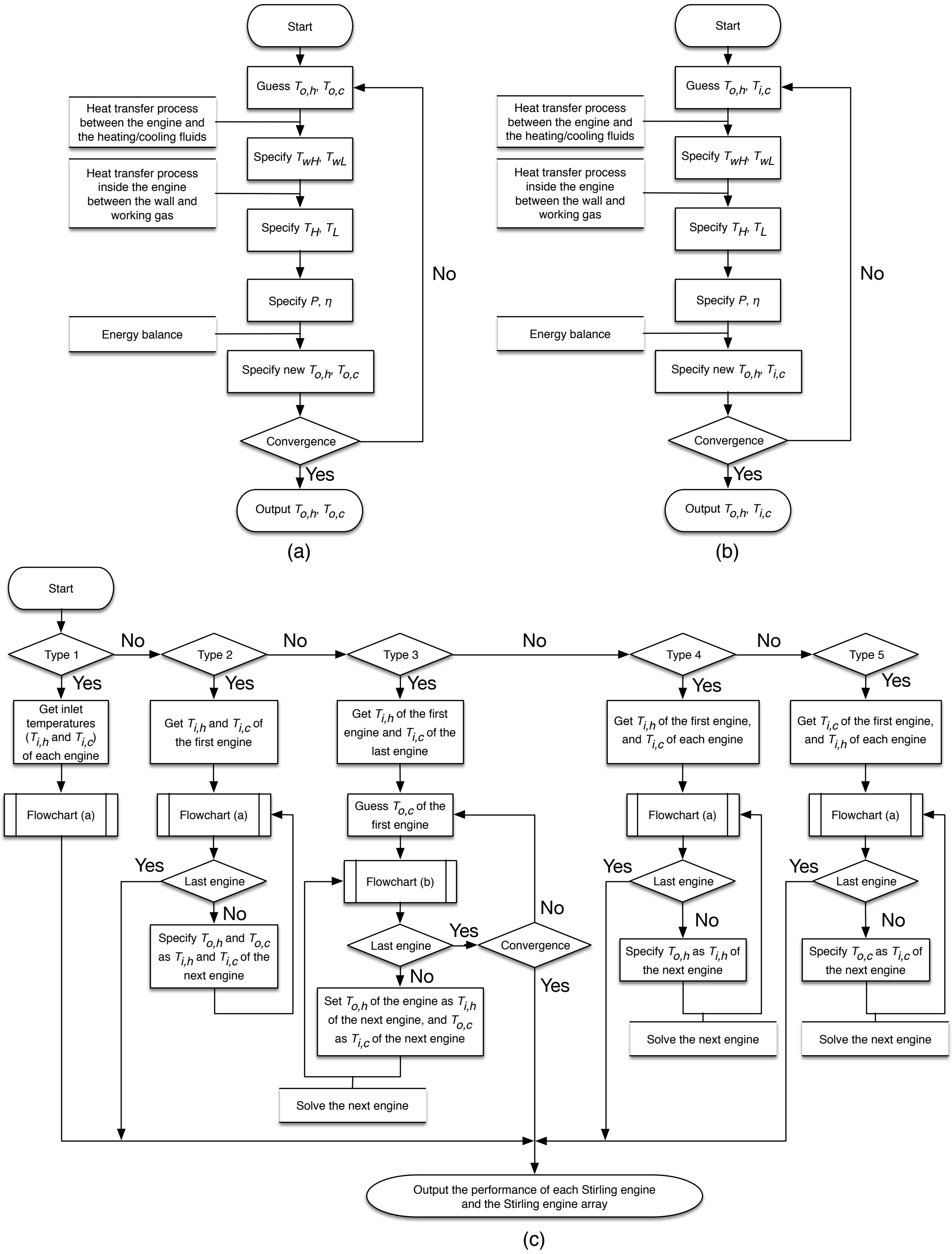

Figure 3-5　Flowcharts of the SEA model for performance analysis of the SEAs

(a) according to the equations derived; similarly, known inlet parameters of heating fluid and outlet parameters of cooling fluid, the performance of a Stirling engine can be obtained from flowchart (b). Flowchart (c) shows the algorithm to solve the SEA model iteratively depending on different connection types. The levenberg-marquardt algorithm is applied to numerically solve the non-linear equations in the flowcharts.

3.8 Result Analysis

SEA models with specified parameters in Table 3.5 were built and calculated. Results are shown in Table 3.6, it can be found that under specified parameters Type 3 has the highest efficiency and output power, while Type 1 has the lowest efficiency and output power.

Table 3.6 Results of SEA models under specified parameters

Parameter	Value	Parameter	Value
η_1	0.2215	P_1	8022 W
η_2	0.2273	P_2	8483 W
η_3	0.2277	P_3	8512 W
η_4	0.2227	P_4	8116 W
η_5	0.2263	P_5	8399 W

3.8.1 Effectes of $T_{i,h}$

According to Carnot cycle efficiency formula, the temperature of heating fluid determines the efficiency of Stirling engine array. For a Stirling engine, lower temperature heating fluid leads to a lower efficiency. The efficiency and output power may drop to 0 due to its insufficient heating fluid temperature to drive the engine.

Curves of performance of SEAs and $T_{i,h}$ are shown in Figure 3-6. As it is shown, with the increase of $T_{i,h}$, both η and P increase for all SEAs. For some types of SEA, when $T_{i,h}$ is lower than a critical temperature, some of the engines in the SEA will not work and there

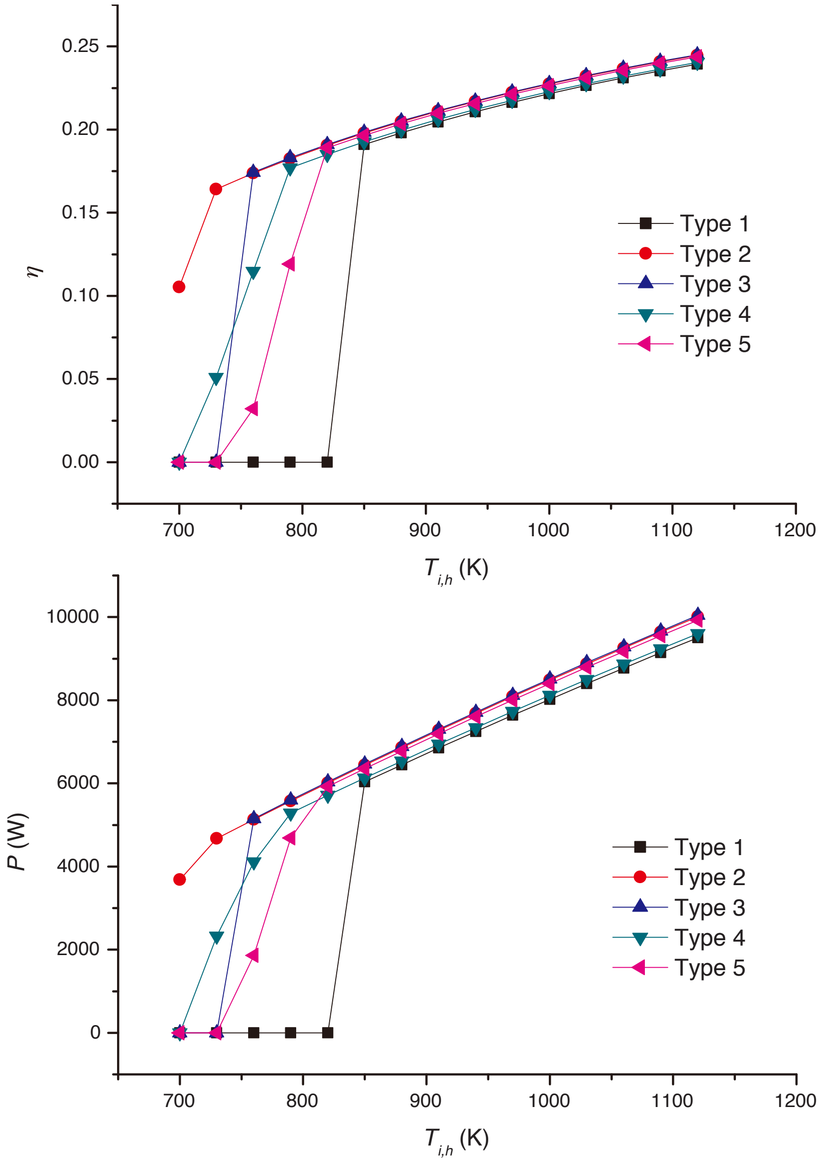

Figure 3-6 Influence of $T_{i,h}$ on efficiency and power of SEA

will be turning points on the $\eta - T_{i,h}$, $P - T_{i,h}$ curves. E.g. for SEA of Type 1, when $T_{i,h}$ is lower 820 K, all the engines stop working, turning points at 820 K can be found on the $\eta - T_{i,h}$, $P - T_{i,h}$ curves in Figure 3-6.

From curves in Figure 3-6, it can be concluded that Type 2 and Type 3 have the best performance, and Type 2 has the best adaptability for lower $T_{i,h}$. All engines in Type 2 begin to work at 730 K.

3.8.2 Effects of $q_m c_p$

According to Equation 3.29, 3.30, $q_m c_p$ (both $q_{m,h} c_{p,h}$ and $q_{m,c} c_{p,c}$) will affect the heat transfer process, which is one of the vital factor for the performance of SEA.

Curves of performance of SEAs and $q_{m,h} c_{p,h}$ are shown in Figure 3-7. For a large $q_{m,h} c_{p,h}$ ($>$ 800 W/K), Type 2 , Type 3 and Type 5 have similar performance, which can be interpreted as the cooling fluid has the same properties for the two types of SEAs, and for a large $q_{m,h} c_{p,h}$, the heating fluid has similar effect after diverged. Similar performance of Type 1 and Type 4 can be also interpreted for the same reason.

Curves of performance of SEAs and $q_{m,c} c_{p,c}$ are shown in Figure 3-8. For a connection type of SEA, the performance improves with the increase of $q_{m,c} c_{p,c}$. For a large $q_{m,c} c_{p,c}$ ($>$ 800 W/K), Type 2 and Type 3 have similar performance, which means the flow order doesn't affect the performance of SEA with a large $q_{m,c} c_{p,c}$. There exists an intersection point (at 830 W/K) of curves of Type 4 and Type 5. For a larger $q_{m,c} c_{p,c}$, Type 4 has a better performance, and vice versa. This can be interpreted that larger $q_{m,c} c_{p,c}$ weaken the drawback of larger temperature rise of parallel flow, while for the heating fluid, temperature drop of serial flow is smaller than parallel flow.

3.8.3 Effects of n_{se}

By varying the number of engines in SEA, the performance levels changed accordingly. n_{se} may affect both the flow rates and temperatures of fluids of each engine. Figure 3-9 shows curves of performance of SEAs with different n_{se}. As it is shown, with an increase of n_{se} leads to a reduction of η for all SEAs due to smaller heating and cooling average temperature difference for more engines. For some types of SEA, when n_{se} is larger than a critical value,

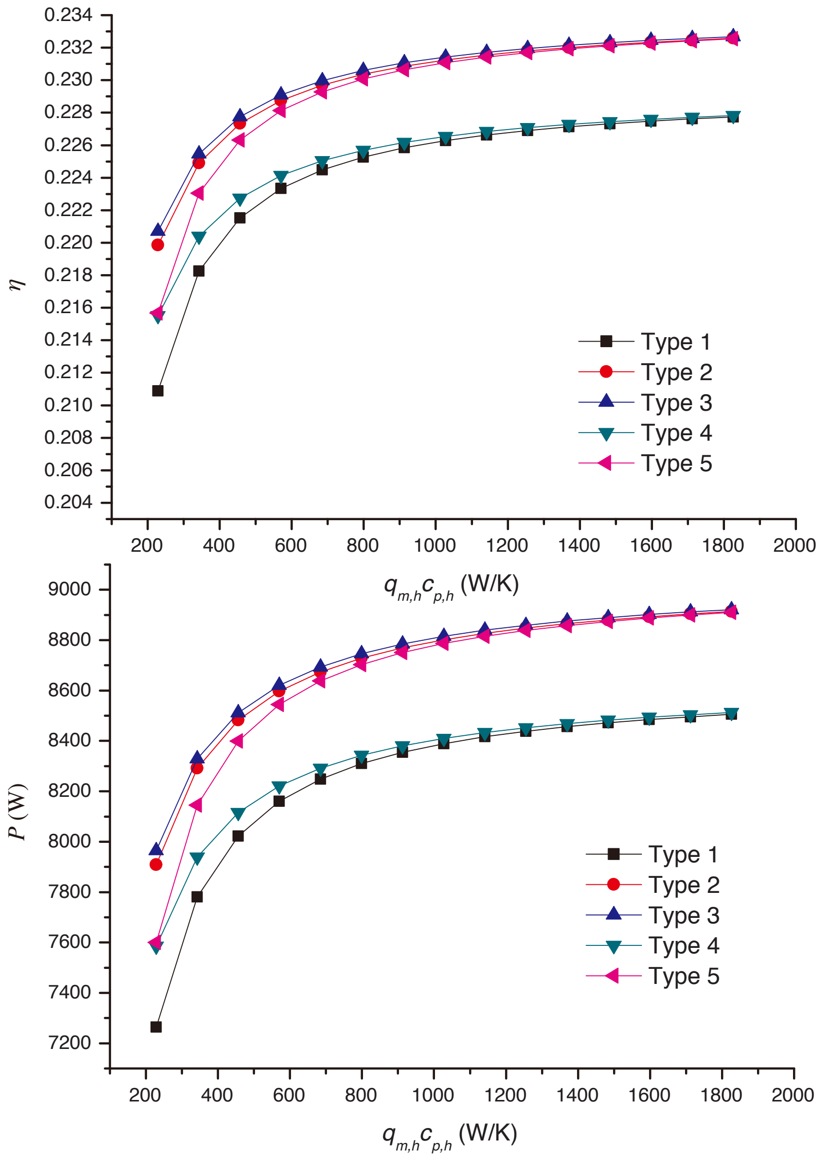

Figure 3-7 Influence of $q_{m,h}c_{p,h}$ on efficiency and power of SEA

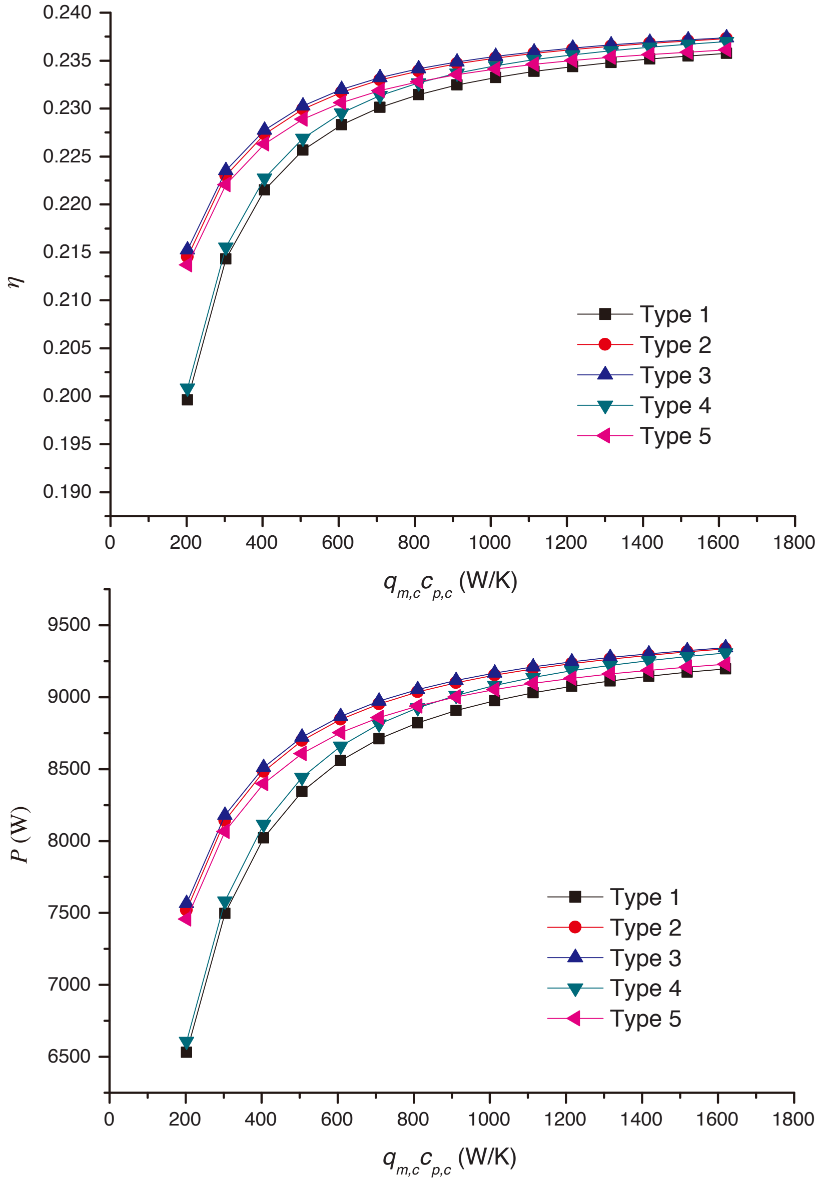

Figure 3-8 Influence of $q_{m,c}c_{p,c}$ on efficiency and power of SEA

some of the engines in the SEA will not work and the curves will dive. E.g. for SEA of Type 1, when n_{se} is larger than 9, all the engines stop working, turning points at 9 can be found on the $\eta - n_{se}$, $P - n_{se}$ curves in Figure 3-9.

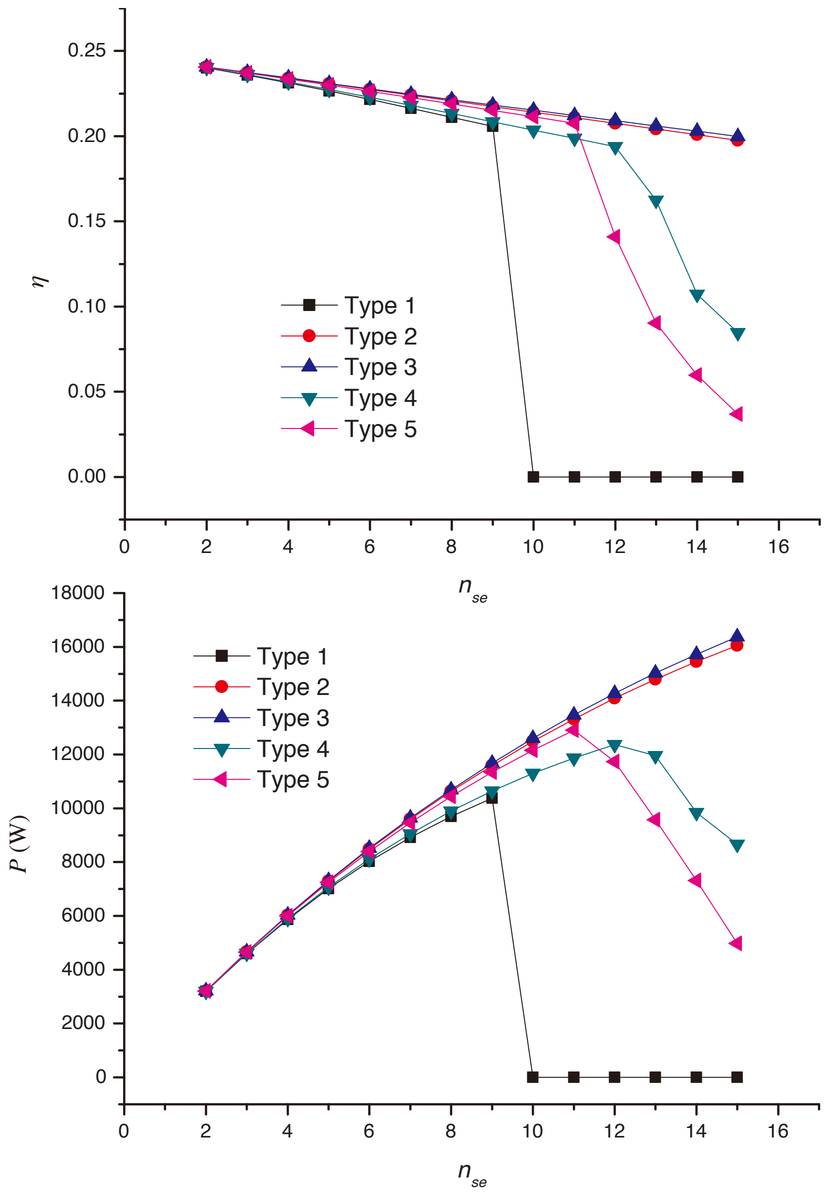

Figure 3-9 Influence of n_{se} on efficiency and power of SEA

For Type 1, when $n_{se} \geqslant 10$, all engines stop working for given heating and cooling fluids due to small $q_m c_p$. For Type 2 and Type 3, every engine in the SEAs works, by increasing n_{se}, η reduces due to smaller temperature difference of the fluids, and P increases due to more operating engines. For Type 4, by checking results, it can be found that when $n_{se} = 13$, the last engine doesn't work; when $n_{se} = 14$, only the first 10 engines will work; when $n_{se} = 15$, the working engine number drops to 9. For Type 5, by checking results, it can be found that when $n_{se} = 12$, the last 2 engines stop working; when $n_{se} = 13$, only the first 8 engines will work; when $n_{se} = 14$, the working engine number drops to 6; when $n_{se} = 15$, the working engine number drops to 4.

3.9 Conclusion

Connection type may change the flow rates and temperatures of the fluids, as a result the performance of the SEA will be different depending on the connection schemes. In order to compare performance of SEAs with different connections, five basic connection types of SEA were summed up according to flow type and flow order.

Analytical Stirling engine model was created to develop the SEA models for the investigation of influence of connection types. Imperfect regeneration and cycle irreversibility of Stirling engine cycle and heat exchange process between fluids and engine were considered in the model. The model was evaluated by considering the prototype GPU-3 Stirling engine as a case study. Result shows that the proposed model predicted the performance with higher accuracy than the previous models. Models of SEAs were developed to calculated the performance under different parameters to find out impacts of $T_{i,h}$, $q_{m,h}c_{p,h}$, $q_{m,c}c_{p,c}$ and n_{se} on different connection types.

It was found that, as expected, decrease $T_{i,h}$ and $q_m c_p$ will weaken the performance of SEA of all connection types. However, for some connection types, there exists a critical temperature below which some engines stop working. This needs to be considered for SEA connection type selection, especially when $T_{i,h}$ is low. For given $T_{i,h}$, $T_{i,c}$ and $q_m c_p$, Type 2 has the best performance and adaptability.

From Figure 3-6-3-9, it can be found that Type 2 and Type 3 have the best performance, while Type 1 has the worst performance. Type 2 and Type 3 have similar performance under different parameters ($T_{i,h}$, $T_{i,c}$ and $q_m c_p$), which means the flow order has little influence on the performance of an SEA.

For a certain connection type, increase n_{se} will reduce the efficiency of SEA. For some connection types, increase n_{se} will reduce the output power P due to inoperative engines and smaller output power engines. Thus it is important to choose the number of engines for some connection types of SEA.

As a conclusion, SEA of serial flows has the best performance and adaptability under different parameters. Given heating and cooling fluids, using serial flow is the best choice for the connection type of an SEA.

It is important to note that, in the future researches, the experiments of influence of connection type on SEA's performance can be carried out to verify the conclusions in this paper.

3.10 Steam Generators

Chapter 4 Conclusions

Acknowledge

This is the acknowledgement part.

Bibliography

[1] Babaelahi M, Sayyaadi H. A new thermal model based on polytropic numerical simulation of Stirling engines. Applied Energy, 2015, 141:143 – 159.

[2] MARTINI W R. Stirling engine design manual, 2nd edition. Technical report, Martini Engineering, Richland, WA (USA), 1983.

[3] Price H, Lupfert E, Kearney D, et al. Advances in Parabolic Trough Solar Power Technology. Journal of Solar Energy Engineering, 2002, 124(2):109–125.

[4] Padilla R V, Demirkaya G, Goswami D Y, et al. Heat transfer analysis of parabolic trough solar receiver. Applied Energy, 2011, 88(12):5097 – 5110.

[5] Mohamad A, Orfi J, Alansary H. Heat losses from parabolic trough solar collectors. International Journal of Energy Research, 2014, 38(1):20–28.

[6] Guo J, Huai X, Liu Z. Performance investigation of parabolic trough solar receiver. Applied Thermal Engineering, 2016, 95:357 – 364.

[7] Guo J, Huai X. Multi-parameter optimization design of parabolic trough solar receiver. Applied Thermal Engineering, 2016, 98:73 – 79.

[8] Padilla R V, Fontalvo A, Demirkaya G, et al. Exergy analysis of parabolic trough solar receiver. Applied Thermal Engineering, 2014, 67(1-2):579 – 586.

[9] Huang W, Hu P, Chen Z. Performance simulation of a parabolic trough solar collector. Solar Energy, 2012, 86(2):746 – 755.

[10] Wang J, Wang J, Bi X, et al. Performance Simulation Comparison for Parabolic Trough Solar Collectors in China. International Journal of Photoenergy, 2016, 2016(18):1–16.

[11] Al-Sulaiman F A. Exergy analysis of parabolic trough solar collectors integrated with combined steam and organic Rankine cycles. Energy Conversion and Management, 2014, 77:441 – 449.

[12] Hachicha A, Rodriguez I, Capdevila R, et al. Heat transfer analysis and numerical simulation of a parabolic trough solar collector. Applied Energy, 2013, 111:581 – 592.

[13] Ashouri M, Vandani A M K, Mehrpooya M, et al. Techno-economic assessment of a Kalina cycle driven by a parabolic Trough solar collector. Energy Conversion and Management, 2015, 105:1328 – 1339.

[14] Guo S, Liu D, Chu Y, et al. Real-time dynamic analysis for complete loop of direct steam generation solar trough collector. Energy Conversion and Management, 2016, 126:573 – 580.

[15] Bader R, Pedretti A, Barbato M, et al. An air-based corrugated cavity-receiver for solar parabolic trough concentrators. Applied Energy, 2015, 138:337 – 345.

[16] Good P, Ambrosetti G, Pedretti A, et al. An array of coiled absorber tubes for solar trough concentrators operating with air at 600°C and above. Solar Energy, 2015, 111:378 – 395.

[17] Boukelia T, Arslan O, Mecibah M. ANN-based optimization of a parabolic trough solar thermal power plant. Applied Thermal Engineering, 2016, 107:1210 – 1218.

[18] Kaloudis E, Papanicolaou E, Belessiotis V. Numerical simulations of a parabolic trough solar col-

lector with nanofluid using a two-phase model. Renewable Energy, 2016, 97:218 – 229.

[19] Tan L, Ji X, Li M, et al. The experimental study of a two-stage photovoltaic thermal system based on solar trough concentration. Energy Conversion and Management, 2014, 86:410 – 417.

[20] Al-Sulaiman F A, Hamdullahpur F, Dincer I. Performance assessment of a novel system using parabolic trough solar collectors for combined cooling, heating, and power production. Renewable Energy, 2012, 48:161 – 172.

[21] Lobon D H, Valenzuela L, Baglietto E. Modeling the dynamics of the multiphase fluid in the parabolic-trough solar steam generating systems. Energy Conversion and Management, 2014, 78:393 – 404.

[22] Xu C, Chen Z, Li M, et al. Research on the compensation of the end loss effect for parabolic trough solar collectors. Applied Energy, 2014, 115:128 – 139.

[23] Liu Q, Yang M, Lei J, et al. Modeling and optimizing parabolic trough solar collector systems using the least squares support vector machine method. Solar Energy, 2012, 86(7):1973 – 1980.

[24] Blázquez R, Carballo J, Silva M. Optical design and optimization of parabolic dish solar concentrator with a cavity hybrid receiver. AIP Conference Proceedings, 2016, 1734(1).

[25] Craig O O, Dobson R T. Parabolic solar cooker: Cooking with heat pipe vs direct spiral copper tubes. AIP Conference Proceedings, 2016, 1734(1).

[26] Qianjun M, Ming X, Yong S, et al. Study on solar photo-thermal conversion efficiency of a solar parabolic dish system. Environmental Progress & Sustainable Energy, 2014, 33(4):1438–1444.

[27] Mawire A, Taole S H. Experimental energy and exergy performance of a solar receiver for a domestic parabolic dish concentrator for teaching purposes. Energy for Sustainable Development, 2014, 19:162 – 169.

[28] Reddy K, Vikram T S, Veershetty G. Combined heat loss analysis of solar parabolic dish – modified cavity receiver for superheated steam generation. Solar Energy, 2015, 121:78 – 93. {ISES} Solar World Congress 2013 (SWC2013) Special Issue.

[29] Reddy K, Natarajan S K, Veershetty G. Experimental performance investigation of modified cavity receiver with fuzzy focal solar dish concentrator. Renewable Energy, 2015, 74:148 – 157.

[30] Vikram T S, Reddy K. Investigation of convective and radiative heat losses from modified cavity based solar dish steam generator using {ANN}. International Journal of Thermal Sciences, 2015, 87:19 – 30.

[31] Sagade A A. Experimental investigation of effect of variation of mass flow rate on performance of parabolic dish water heater with non-coated receiver. International Journal of Sustainable Energy, 2015, 34(10):645–656.

[32] Skouri S, Bouadila S, Salah M B, et al. Comparative study of different means of concentrated solar flux measurement of solar parabolic dish. Energy Conversion and Management, 2013, 76:1043 – 1052.

[33] Uma Maheswari C, Meenakshi Reddy R. CFD Analysis of a Solar Parabolic Dish. Applied Mechanics & Materials, 2015, 787:280–284.

[34] Patil P N, Khandekar M A, Patil S N. Automatic dual-axis solar tracking system for parabolic dish. in: Proceedings of 2016 2nd International Conference on Advances in Electrical, Electronics, Information, Communication and Bio-Informatics (AEEICB), Feb, 2016, 699-703.

[35] PAVLOVIĆ S R, STEFANOVIĆ V P, SULJKOVIĆ S H. OPTICAL MODELING OF A SOLAR DISH THERMAL CONCENTRATOR BASED ON SQUARE FLAT FACETS. Thermal Science, 2014, 18(3):989 – 998.

[36] Senft J R. Theoretical limits on the performance of stirling engines. International Journal of Energy Research, 1998, 22(11):991–1000.

[37] Costea M, Petrescu S, Harman C. The effect of irreversibilities on solar Stirling engine cycle performance. Energy Conversion and Management, 1999, 40(15–16):1723 – 1731.

[38] Prieto J I, Stefanovskiy A B. Dimensional analysis of leakage and mechanical power losses of kinematic Stirling engines. Proceedings of the Institution of Mechanical Engineers, Part C: Journal of Mechanical Engineering Science, 2003, 217(8):917–934.

[39] Organ A J. Stirling Cycle Engines : Inner Workings and Design (1). Somerset, GB: Wiley, 2013.

[40] Kongtragool B, Wongwises S. Investigation on power output of the gamma-configuration low temperature differential Stirling engines. Renewable Energy, 2005, 30(3):465 – 476.

[41] Thombare D, Verma S. Technological development in the Stirling cycle engines. Renewable and Sustainable Energy Reviews, 2008, 12(1):1 – 38.

[42] Ohtomo M, Isshiki N. Basic Performance of a Three-Temperature Stirling Cycle Machine Using Vector Analysis. Nihon Kikai Gakkai Ronbunshu B Hen/transactions of the Japan Society of Mechanical Engineers Part B, 1995, 61(591):4219–4225.

[43] Rogdakis E, Bormpilas N, Koniakos I. A thermodynamic study for the optimization of stable operation of free piston Stirling engines. Energy Conversion and Management, 2004, 45(4):575 – 593.

[44] Kongtragool B, Wongwises S. Thermodynamic analysis of a Stirling engine including dead volumes of hot space, cold space and regenerator. Renewable Energy, 2006, 31(3):345 – 359.

[45] Puech P, Tishkova V. Thermodynamic analysis of a Stirling engine including regenerator dead volume. Renewable Energy, 2011, 36(2):872 – 878.

[46] Formosa F, Despesse G. Analytical model for Stirling cycle machine design. Energy Conversion and Management, 2010, 51(10):1855–1863.

[47] Shazly J, Hafez A, Shenawy E E, et al. Simulation, design and thermal analysis of a solar Stirling engine using MATLAB. Energy Conversion and Management, 2014, 79:626 – 639.

[48] Cullen B, McGovern J. Development of a theoretical decoupled Stirling cycle engine. Simulation Modelling Practice and Theory, 2011, 19(4):1227 – 1234. Sustainable Energy and Environmental Protection “SEEP2009”.

[49] Ahmadi M H, Sayyaadi H, Dehghani S, et al. Designing a solar powered Stirling heat engine based on multiple criteria: Maximized thermal efficiency and power. Energy Conversion and Management, 2013, 75:282 – 291.

[50] Ahmadi M H, Sayyaadi H, Mohammadi A H, et al. Thermo-economic multi-objective optimization of solar dish-Stirling engine by implementing evolutionary algorithm. Energy Conversion and Management, 2013, 73:370 – 380.

[51] Tursunbaev I A. Analytic model of solar power plant with a Stirling engine. Applied Solar Energy, 2007, 43(1):13–16. 版权 - Allerton Press, Inc. 2007; 最近更新 - 2014-08-30.

[52] Urieli I, Berchowitz D M. Stirling cycle engine analysis. Bristol: A. Hilger, 1984.

[53] Ni M, Shi B, Xiao G, et al. Improved Simple Analytical Model and experimental study of a 100 W beta-type Stirling engine. Applied Energy, 2016, 169:768 – 787.

[54] Jia B, Smallbone A, Feng H, et al. A fast response free-piston engine generator numerical model for control applications. Applied Energy, 2016, 162:321 – 329.

[55] Strauss J M, Dobson R T. Evaluation of a second order simulation for Sterling engine design and optimisation. Journal of Energy in Southern Africa, 2010, 21(2):17–29.

[56] Abbas M. Thermal analysis of Stirling engine solar driven. Cder Dz, 2014, 70(3):503–514.

[57] Araoz J A, Salomon M, Alejo L, et al. Numerical simulation for the design analysis of kinematic Stirling engines. Applied Energy, 2015, 159:633 – 650.

[58] Barreto G, Canhoto P. Modelling of a Stirling engine with parabolic dish for thermal to electric conversion of solar energy. Energy Conversion and Management, 2017, 132:119 – 135.

[59] Wu F, Chen L, Wu C, et al. Optimum performance of irreversible stirling engine with imperfect regeneration. Energy Conversion and Management, 1998, 39(8):727 – 732.

[60] Yaqi L, Yaling H, Weiwei W. Optimization of solar-powered Stirling heat engine with finite-time thermodynamics. Renewable Energy, 2011, 36(1):421 – 427.

[61] Hosseinzade H, Sayyaadi H, Babaelahi M. A new closed-form analytical thermal model for simulating Stirling engines based on polytropic-finite speed thermodynamics. Energy Conversion and Management, 2015, 90:395 – 408.

[62] Ahmadi M H, Ahmadi M A, Pourfayaz F, et al. Optimization of powered Stirling heat engine with finite speed thermodynamics. Energy Conversion and Management, 2016, 108:96 – 105.

[63] Chen L, Zhang W, Sun F. Power, efficiency, entropy-generation rate and ecological optimization for a class of generalized irreversible universal heat-engine cycles. Applied Energy, 2007, 84(5):512 – 525.

[64] Ahmadi M H, Ahmadi M A, Mellit A, et al. Thermodynamic analysis and multi objective optimization of performance of solar dish Stirling engine by the centrality of entransy and entropy generation. International Journal of Electrical Power & Energy Systems, 2016, 78:88 – 95.

[65] Li R, Grosu L, Queiros-Conde D. Multi-objective optimization of Stirling engine using Finite Physical Dimensions Thermodynamics (FPDT) method. Energy Conversion and Management, 2016, 124:517 – 527.

[66] Patel V, Savsani V. Multi-objective optimization of a Stirling heat engine using TS-TLBO (tutorial training and self learning inspired teaching-learning based optimization) algorithm. Energy, 2016, 95:528 – 541.

[67] Luo Z, Sultan U, Ni M, et al. Multi-objective optimization for GPU3 Stirling engine by combining multi-objective algorithms. Renewable Energy, 2016, 94:114 – 125.

[68] Cheng Z, He Y, Cui F. A new modelling method and unified code with MCRT for concentrating solar collectors and its applications. Applied Energy, 2013, 101:686 – 698. Sustainable Development of Energy, Water and Environment Systems.

[69] Mao Q, Shuai Y, Yuan Y. Study on radiation flux of the receiver with a parabolic solar concentrator system. Energy Conversion and Management, 2014, 84:1 – 6.

[70] Wang M, Siddiqui K. The impact of geometrical parameters on the thermal performance of a solar receiver of dish-type concentrated solar energy system. Renewable Energy, 2010, 35(11):2501 –

2513.

[71] Wang F, Shuai Y, Tan H, et al. Heat transfer analyses of porous media receiver with multi-dish collector by coupling MCRT and FVM method. Solar Energy, 2013, 93:158 – 168.

[72] Zhu J, Wang K, Wu H, et al. Experimental investigation on the energy and exergy performance of a coiled tube solar receiver. Applied Energy, 2015, 156:519 – 527.

[73] Li S, Xu G, Luo X, et al. Optical performance of a solar dish concentrator/receiver system: Influence of geometrical and surface properties of cavity receiver. Energy, 2016, 113:95 – 107.

[74] Daabo A M, Mahmoud S, Al-Dadah R K. The effect of receiver geometry on the optical performance of a small-scale solar cavity receiver for parabolic dish applications. Energy, 2016, 114:513 – 525.

[75] Loni R, Kasaeian A, Asli-Ardeh E A, et al. Performance study of a solar-assisted organic Rankine cycle using a dish-mounted rectangular-cavity tubular solar receiver. Applied Thermal Engineering, 2016, 108:1298 – 1309.

[76] Wang W, Xu H, Laumert B, et al. An inverse design method for a cavity receiver used in solar dish Brayton system. Solar Energy, 2014, 110:745 – 755.

[77] Craig K J, Marsberg J, Meyer J P. Combining ray tracing and CFD in the thermal analysis of a parabolic dish tubular cavity receiver. AIP Conference Proceedings, 2016, 1734(1).

[78] Aichmayer L, Spelling J, Laumert B. Preliminary design and analysis of a novel solar receiver for a micro gas-turbine based solar dish system. Solar Energy, 2015, 114:378 – 396.

[79] Lovegrove K, Luzzi A, Soldiani I, et al. Developing ammonia based thermochemical energy storage for dish power plants. Solar Energy, 2004, 76(1–3):331 – 337. Solar World Congress 2001.

[80] Organ A J. The Regenerator and the Stirling Engine. Mechanical Engineering Publications Limited, 1997.

[81] Juhasz A. A mass computation model for lightweight brayton cycle regenerator heat exchangers. in: Proceedings of 8th Annual International Energy Conversion Engineering Conference, 2010.

[82] Duan C, Wang X, Shu S, et al. Thermodynamic design of Stirling engine using multi-objective particle swarm optimization algorithm. Energy Conversion & Management, 2014, 84:88–96.

[83] Heywood, JohnB. Internal combustion engine fundamentals. McGraw-Hill, 1988.

[84] Timoumi Y, Tlili I, Nasrallah S B. Design and performance optimization of GPU-3 Stirling engines. Energy, 2008, 33(7):1100 – 1114.

[85] Hooshang M, Moghadam R A, AlizadehNia S. Dynamic response simulation and experiment for gamma-type Stirling engine. Renewable Energy, 2016, 86:192 – 205.

Appendix A Publication

[1] Zhang Cheng, Kun Wang. International Conference on Power Engineering: ICOPE 2013: FEA simulation on the alignment of the shafts of three-fulcrum turbine.

[2] Performance comparison of new and traditional arrangements of a dish-Stirling system

[3] A multi-stage exergy-loss reduction system for solar parabolic trough power plants

[4] Cascade system using both trough system and dish system for power generation

[5] A solar thermal cascade system, No. 201610806296.5

[6] A flow control method used in a multi-stage heating system, No. 201610805604.2

Appendix B　Formulae

The is the content of the Appendix B